Performance Analysis Of Hybrid Metal-Graphene Frequency Reconfigurable Antennas In The Microwave Regime

Performance Analysis Of Hybrid Metal-Graphene Frequency Reconfigurable Antennas In The Microwave Regime

Christian Nñez Alvarez, *Member, IEEE*, Rebecca Cheung, *Senior Member, IEEE*, and John S. Thompson, *Fellow, IEEE*

***Abstract*—This paper analyses the potential application of graphene in microwave frequency reconfigurable antennas. Two multi-band designs, one for wireless local area networks (WIFI), covering the frequency bands of 2.4 GHz, 3.6 GHz and 5 GHz; and another for the cellular long term evolution (LTE) system, operating the frequency bands of 1.8 GHz, 2.5 GHz, 2.6 GHz and 3.6 GHz; are evaluated to demonstrate the working principle and the performance trade-offs. The designs are made mostly of copper with some parts made of graphene to enable reconfigurable behaviour. The graphene material's surface impedance is tuned by applying a DC bias voltage which allows to obtain one of two extreme values that emulate the ON and OFF states of common switches such as Micro Electromechanical Switches (MEMS), Field effect transistor (FET) and P-type Insulator N-type (PIN) diode, or continuous values to mimic reconfigurable antennas loaded by varactors. This material switching modifies the electrical length of the current propagating through the antenna and consequently switches the resonant frequencies. Additionally, results show that hybrid metal-graphene frequency reconfigurable antennas can, at the same time, provide tunable bandwidth and antenna matching.**

***Index Terms*—Microstrip antennas, microwave antennas, multifrequency antennas, switching frequency.**

I. INTRODUCTION

Future wireless devices will incorporate multiple wireless services operating over a wide frequency spectrum such as 3^{rd} (3G) and 4^{th} (4G) mobile generation and beyond at 700-800 MHz, 1.8-2.6 GHz and 3.6 GHz; wireless fidelity (WIFI) at 2.4 GHz, 3.6 GHz and 5 GHz. In order to shrink a multi-radio transmitting system, antenna reconfiguration provides an option to integrate multiple radiating elements at different frequencies into a single physical antenna, and hence, save space.

A reconfigurable antenna is designed in a manner that it is possible to manually or automatically (via software) change its resonant frequency, operational bandwidth, radiation pattern, and/or polarization to adapt to different services, system requirements and the environment. This is most commonly done with Micro or Nano Electromechanical systems (MEMS or NEMS) [1], [2], electrical RF switches such as Metal Semiconductor Field Effect Transistor (MESFET) and Pseudomorphic High Electron Mobility transistor (PHEMT) [3], [4], diode-based technology such as the P-type Insulator N-type diode (PIN diode) [5], [6], varactors [7], [8] or tunable materials [9]; via applying a mechanical, electrical, magnetic, light or thermal bias [10]. Alternatively, the tunable surface impedance of graphene can also be used as tunable material in reconfigurable antennas.

Graphene is a flat mono-atomic layer of Carbon atoms distributed in a two-dimensional honeycomb-like lattice [11]. In addition, an unbiased pristine single layer of graphene (SLG) only absorbs 2.3% [12] of visible light and supports breaking forces of up to 42 N/m with a Young's modulus of 1 TPa and an intrinsic strength of 130 GPa [13] while also being extremely light (0.77 mg/m^2). As a result, a reconfigurable antenna made of graphene could also be transparent, flexible and light weight. Importantly, the admittance of graphene can be tuned by applying an electrostatic field perpendicular to the graphene layer, or in other words, by applying a DC voltage bias, and hence, high and low impedances can be set to mimic the ON and OFF states found in switches. This effect is used in the present paper to affect the currents propagating in the antenna, and consequently, change the resonant frequency. However, graphene is not only an alternative option to a conventional RF switch, it can be used for fabricating the radiating antenna itself.

Graphene reconfigurable antennas are being mostly

This work was supported by the Engineering and Physical Sciences Research Council (EPSRC) grant no. EP/K503034/1. Data from this work can be accessed from the University of Edinburgh in http://hdl.handle.net/10283/2219. Color versions of one or more of the figures in this paper are available online at http://ieeexplore.ieee.org.

C. Nuñez Alvarez and J. S. Thompson are with the Institute for Digital Communications (IDCOM), the University of Edinburgh, EH9 3JL, UK. (e-mail: cnuneza@staffmail.ed.ac.uk)

R. Cheung is with the Institute for Integrated Micro- and Nano-Systems (IMNS), the University of Edinburgh, EH9 3FF, UK.

studied for infra-red and THz frequencies as graphene can significantly reduce size and provide high antenna reconfigurability at such frequencies [14]–[21]. In [22], the authors studied the performance of wearable antennas made of graphene ink from 1 GHz to 5 GHz. The resonant frequency, bandwidth and gain of the antennas in their study were slightly affected by bending and twisting. The proposed antennas in this paper might produce enough reconfigurability to compensate for these effects observed in the graphene ink case. Since antennas fully made of graphene are expected to have low antenna efficiencies with very little reconfigurability at microwave frequencies [15], [23], the antenna designs proposed here are hybrid metal-graphene frequency reconfigurable antennas where the impact of the high ohmic losses of graphene is reduced while providing substantial antenna reconfigurability. In [24], the concept and analysis of hybrid metal-graphene antennas were introduced for THz frequencies. However, as large area samples of graphene grown by chemical vapour deposition (CVD) have been successfully synthesised [25], this paper carries out a feasibility study of using this novel material as a potential solution for hybrid metal-graphene antennas in the microwave regime. An early work containing similar designs had been presented in [26]. In this paper, a deeper and more detailed analysis on related hybrid metal-graphene frequency reconfigurable antenna designs is presented.

The novel contributions of this paper can be summarized as follows:

- Analyse and simulate two possible hybrid metal-graphene reconfigurable antenna designs to cover WIFI (2.4 GHz, 3.6 GHz and 5 GHz) and LTE (1.8 GHz , 2.1 GHz , 2.6 GHz and 3.6 GHz) frequency bands.
- Present the advantages and disadvantages of using graphene in reconfigurable antennas at microwave frequencies as well as system limitations such as the selection of suitable dielectric-semiconductor layers for the DC voltage bias and the power consumption.

The paper is structured as follows, sections II and III will introduce the admittance of graphene and system limitations, then, section IV will define the proposed antenna designs and the system set up. Afterwards, the simulation results are presented and discussed in section V. Finally, section VI will finish the paper with key conclusions.

II. ADMITTANCE PROPERTIES OF GRAPHENE

For the range of frequencies considered in this paper and in the absence of magnetic field B, the graphene's dynamic, or alternating current (AC), surface admittance σ_{AC} can be evaluated in a Kubo-like form in equation (1) [27], [28]

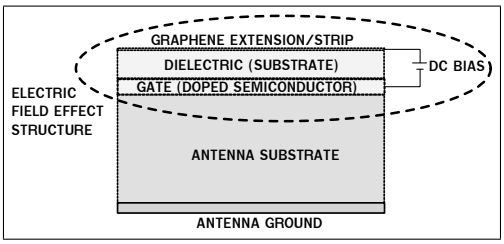

Fig. 1: Example of an electric field effect structure added to a patch antenna.

$$\sigma_{AC} \approx \frac{-jq^2 k_B T}{\pi\hbar^2(\omega - j\tau_t^{-1})}\left(\frac{\mu_c}{k_B T} + 2\ln(e^{-\frac{\mu_c}{k_B T}} + 1)\right), \tag{1}$$

where ω is the angular frequency $2\pi f$ (rad/s), f is the operating frequency (Hz), μ_c is the chemical potential (J), τ_t is the relaxation time (s) which is assumed to be independent of the energy ζ [28], T is the temperature (K), q is the elementary charge (C), $\hbar$ is the reduced Planck's constant (Js) and k_B is the Boltzmann constant (J/K). In graphene, the chemical potential μ_c is related to the carrier density n (m^{-2}) as shown in equation (2) [11], [29]

$$\mu_c \simeq \hbar v_f \sqrt{n\pi}, \tag{2}$$

where $v_f = 1 \times 10^6$ is the Fermi velocity (m/s) in graphene. The value of n can be dynamically modified via the electric field effect shown in Fig. 1, where a direct current (DC) voltage is applied between a graphene sheet and a heavily doped semiconductor to induce an increment or decrement of the number of charge carriers n in the graphene sheet. In this paper, this electric field effect structure is integrated on the antenna substrate. The change of n follows equation (3) [29], [30]

$$n = \frac{\epsilon_o \epsilon V_b}{dq}, \tag{3}$$

where ϵ_o is the vacuum permittivity (F/m), V_b is the DC voltage bias (V), d is the thickness (m) and ϵ is the relative permittivity of the dielectric separating the graphene sheet and the back gate material (a p or n doped semiconductor).

The total relaxation time τ_t in equation (1) depends on different scattering mechanisms at different carrier densities and temperatures [11], [31]. The Matthiessen rule, equation (4), determines the overall relaxation time τ_t for any carrier density n and temperature T [29],

$$\frac{1}{\tau_t} \simeq \left(\frac{1}{\tau_L}\right) + \left(\frac{1}{\tau_S}\right), \tag{4}$$

where τ_L is due to long range scattering mechanisms such as defects and inpurities, and τ_S is due to short range scattering mechanisms such as phonon and carrier-carrier interactions.

Finally, at room temperature (295 K), the minimum achievable chemical potential μ_{min} is limited by electron-hole puddles caused by charged impurities [32] and can be calculated as follows

$$\zeta_{puddle} \simeq \mu_{c,min} \simeq \hbar v_f \sqrt{\pi \tilde{n}}, \tag{5}$$

where $\tilde{n}$ is the carrier density variations - carrier inhomogeneity density - caused by the electron-hole puddles (m^{-2}) which forces the minimum carrier density n to be greater than or equal to this value $n_{min} \geq \tilde{n}$.

III. SYSTEM LIMITATIONS

In this section, three critical issues are discussed related to the implementation of graphene, and the field-effect structure, in antennas for frequency reconfigurability. In subsection III-A, there is a discussion of the trade-offs between suspending graphene on air or depositing it on a dielectric/substrate, see Fig. 1, and in case of depositing graphene on a substrate, to select a suitable dielectric/substrate material that could provide the best performance. Afterwards, a brief analysis of the effect of adding the heavily doped semiconductor to the antenna structure is found in subsection III-B. Finally, the instantaneous power consumption expression, when a graphene sheet is switched between large or small surface impedances Zs=σ_{AC}^{-1}, is derived in subsection III-C. These points are important for supporting later the selection of the parameters in section IV as well as the power consumed by the proposed antennas in section V.

A. SUSPEND GRAPHENE IN AIR OR DEPOSIT IT ON A SUBSTRATE?

Suspending graphene in air provides better performance than over substrates [33]. However, large electric fields and narrow distances d between the gate semiconductor and graphene sheet, see Fig. 1, are needed to induce high carrier density n values with reasonably low voltages V_b values. This might not be possible to achieve for suspended graphene without compromising its structural integrity [13], [33]. Consequently, only graphene laid on a substrate acting as a dielectric (Fig. 1) is considered from now on.

Recently, CVD grown graphene has also been successfully transferred to hexagonal boron nitride (hBN) substrates providing qualities close to exfoliated graphene and mobilities similar to suspended graphene [34]. Therefore, in this paper, it is assumed that a large area of graphene sheet could be deposited onto hBN substrates following, for instance, the dry method described in [34] in the near future.

B. DOPED SEMICONDUCTOR EFFECT

Heavily doped semiconductors can potentially provide reasonably good values of conductivity, specially in the microwave regime. From the general Drude's formula of conductivity, the conductivity of a doped semiconductor σ_{DS} (S/m) is

$$\sigma_{DS} = n_{DS} q \mu_{DS}, \tag{6}$$

where q is the electron charge (C), n_{DS} (m^{-3}) and μ_{DS} (m^2/Vs) are the free carrier density and mobility of the doped semiconductor respectively. Therefore, by substantially raising the free carrier density n_{DS} (assuming the electron mobility μ_{DS} is kept the same) the conductivity of the doped semiconductor is also highly increased. To compensate this effect, a low carrier mobility μ_{DS} should be selected. As shown later in this paper in Table II, the number of free carrier densities needed in graphene are n_{ON}=5·10^{17} m^{-2} for the ON state and n_{OFF}=6·10^{14} m^{-2} for the OFF state. Consequently, the required free carrier density n_{DS} in the doped semiconductor can be obtained as

$$n_{DS} \geq \frac{(n_{ON} - n_{OFF})}{t_{DS}}, \tag{7}$$

where t_{DS} (m) is the thickness of the doped semiconductor layer. Note that, to reach this relation, the length l (m) and the width w (m) of both, the graphene layer and the doped semiconductor, are assumed to be the same. From equations (6) and (7), the total resistance of the doped semiconductor R_{DS} can be calculated as

$$R_{DS} \leq (\sigma_{DC})^{-1} \frac{l}{w t_{DS}} = \frac{l}{(n_{ON} - n_{OFF})\, w q \mu_{DS}}. \tag{8}$$

For the size of the graphene sheets considered in this paper, see Tables III and IV, and to obtain resistances R_{DS} on the order of kΩ or larger, the required electron mobility should be μ_{DS} ≤0.02 m^2/Vs. Heavily doped silicon carbride (SiC) [35] or hydrogenated amorphous silicon (a-Si:H) [36] can meet these requirements and be used as heavily doped semiconductors in Fig. 1 without a noticable impact on the antenna performance.

Alternatively, the graphene layer could be self-biased. In [37], the authors produced a field-effect structure composed by two doped graphene monolayers at THz frequencies. There, the authors applied one or two different DC voltage bias levels to control independently the surface impedance of each of the doped graphene layers. Applying a similar procedure here but at microwave frequencies would allow one to substitute the doped semicondcutor in Fig. 1 for a doped graphene layer. It is important that this second graphene layer should present low quality (low electron mobility) and hence reduce undesired effects on the antenna performance.

C. DC INSTANTANEOUS POWER IN BIASED GRAPHENE

Finally, another important system limitation is set by the power consumed. In the field effect configuration, Fig. 1, the graphene sheet and the heavily doped semiconductor might be modelled as a parallel plate capacitor. The capacitance C (F) created is defined as

$$C = \frac{\epsilon \epsilon_o A}{d}, \tag{9}$$

where A is the area of the graphene sheet and the doped semiconductor ($l \times w$, assumed to be the same) (m^2). Hence, the resulting capacitance C is dictated, in one hand, by the parameters ϵ and d in equation (3) as low V_b values are desired, and on the other hand, by the dimensions of the graphene sheets used. Although the DC power consumption in capacitors is negligible due to electrical isolation, there is still movement of induced charges between the plates every time the DC bias voltage V_b is changed. This movement of charges creates a temporary current that charges the capacitor and therefore power is dissipated in any resistance present in the circuit. The peak power is the dynamic power (W) consumed by the circuit at t=0 and depends on the transitional current and the voltage on the resistance R present in the circuit - $i_R(t)$ and $v_R(t)$ - as equation (10) shows

$$p(t) = v_R(t) i_R(t) = \left. \frac{V_b^2}{R} e^{\frac{-2t}{\tau_{RC}}} \right|_{t=0} = \frac{n^2 q^2 d A}{\epsilon_o \epsilon \tau_{RC}}. \tag{10}$$

where $\tau_{RC} = RC$ and V_b is obtained from equation (3). This is the maximum power that the circuit might consume at the instant of changing the value of V_b. As observed, a fast switching time causes a large current in the system and more power is consumed during a short amount of time. In contrast, a longer waiting time reduces the maximum power consumed during the charging-discharging time. The value at P_{peak} can be further decreased by using a larger ϵ or reducing the thickness d of the dielectric. This would additionally reduce the required V_b. However, these parameters are not easily modified as ϵ depends on the properties of the target dielectric substrate and d on current technology constraints.

IV. PROPOSED ANTENNA DESIGNS

In order to demonstrate the use of graphene in frequency reconfigurable antennas, two main designs are studied:

- A rectangular microstrip antenna with extensions made of graphene added at the edges, Fig. 2a.
- A rectangular microstrip antenna with inserted strips made of graphene, Fig. 2b.

The first design (Fig. 2a) aims to increase or decrease the physical length of the structure in the ON or OFF state respectively, while the second one (Fig. 2b) diverts the current propagating along the antenna so the effective length is larger or shorter than the physical length in the OFF or ON state respectively. The DC voltage bias (V_b) could be applied directly through the feeding port if a common value of V_b is desired for all the graphene extensions/strips so that it activates and deactivates them all at the same time. That would save the necessity of adding a DC bias circuit. However, inserting a gap between the main patch and the extensions/strips provides a solution to avoid a common DC bias voltage throughout the antenna and allows individual control to activate and deactivate single extensions/strips. Consequently, different DC voltage bias (i.e. Vb_1 and Vb_2) should be applied through individual DC vias lines to each of the required graphene sheets. Figs. 2a and 2c include an example of how the DC vias lines can be implemented. Note that both the DC vias lines in Fig. 2a and the field-effect structure in Fig. 2c have not been included in the simulations due to their extremely small thicknesses (in the nanometre scale). The values of Zs_{ON}, Zs_{OFF} and the general set up values for the simulations are defined next.

A. ELECTRIC FIELD EFFECT CONFIGURATION

For the values shown in Table I, it is firstly assumed that the time between switching from one operating frequency to another does not have to be fast (on the order of 1 millisecond). This is within a reasonable assumption considering handover interruption times in LTE-advanced (60 ms) [38]. The switching time is defined as the time needed for the voltage between the graphene sheet and the semiconductor to rise from 50% of the final value to the 90% [10]. Secondly, the

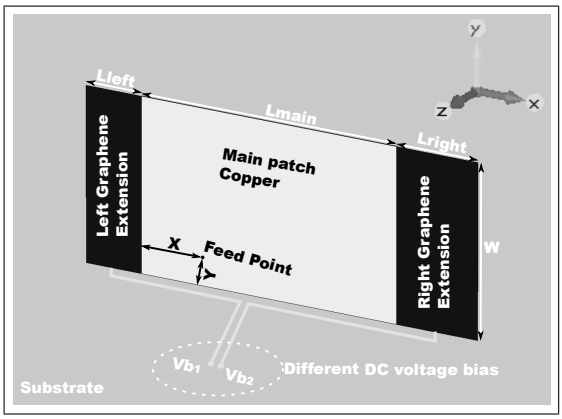

(a)

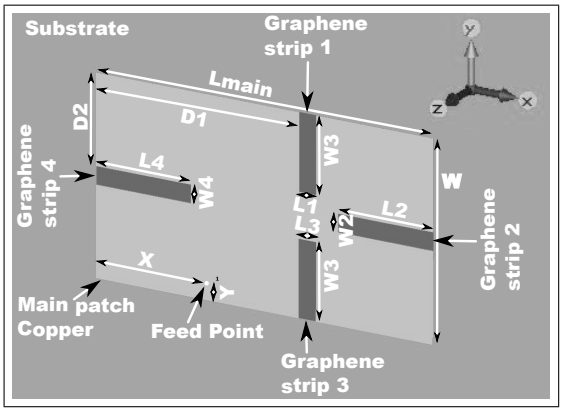

(b)

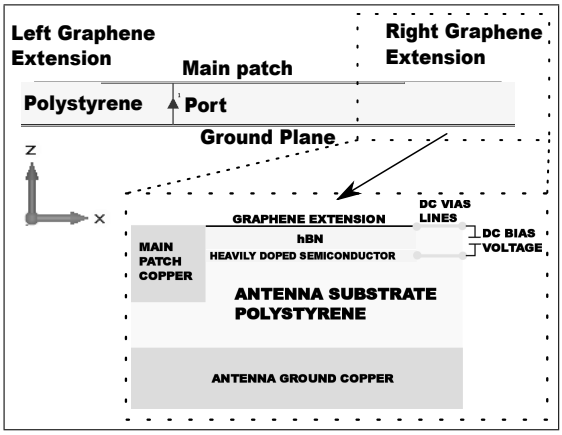

(c)

Fig. 2: Graphical representation of the frequency reconfigurable antennas for a) WIFI applications, b) LTE applications and c) zoomed view of the tuning structure for WIFI design (x-z plane) in a).

thickness d of the dielectric can be reduced up to a few nanometres which is technologically available nowadays [39]. Finally, the ϵ for hBN is obtained from [39].

TABLE I: Selected general parameters

τ_{RC} [ms]	1
Switching time [ms]	1.6
d [nm]	10
ϵ for hBN	4

B. SIMULATED Zs_{ON} AND Zs_{OFF} VALUES

In order to obtain practical values of the ON and OFF state surface impedances Zs_{ON} and Zs_{OFF}, realistic values of τ_S, τ_L and $\tilde{n}$ are needed. Additionally, a high OFF/ON ratio (Zs_{OFF}/Zs_{ON}) is also desired. The values of surface impedance for the ON and OFF states, Zs_{ON} and Zs_{OFF} respectively, in Table II are obtained from equation (11),

$$Zs \approx \frac{j\pi\hbar^2(2\pi f(\tau_L\tau_S) - j(\tau_L + \tau_S))}{q^2(\tau_L\tau_S)[\mu_c + 2k_BT\ln(e^{-\frac{\mu_c}{k_BT}} + 1)]}, \quad (11)$$

where τ_L accounts for all the long range scattering effects and can be calculated as [11], [30], [40]

$$\tau_L = \frac{\mu_L m*}{q} \simeq \frac{\mu_L\hbar\sqrt{n\pi}}{qv_f}, \quad (12)$$

where μ_L is the electron mobility (m^2/Vs) and $m*$ is the carrier mass (Kg) in graphene. Note that equation (11) is a modified version of equation (1) to account for the relaxation time given in equation (4). The value of τ_S is calculated as in equation (13) by just considering the LA phonon contribution, considered in this paper to be the dominant scattering mechanism at room temperature [31], [41], [42],

$$\tau_S = \frac{\mu_p\hbar\sqrt{n\pi}}{qv_f} = \frac{4\hbar^2\rho_m v_{ph}^2 v_f}{\sqrt{n\pi}D^2k_BT}, \quad (13)$$

where D is the deformation potential (eV), $\rho_m = 7.6 \times 10^{-7}$ is the two dimensional mass density of graphene (Kg/m^2) and $v_{ph} = 2.1 \times 10^4$ is the sound velocity of LA phonons in graphene (m/s). The precise deformation potential D value is still discussed, but some experimental values have been obtained in the literature and D $\sim$18 eV seems to be a common and accepted value for graphene over a substrate [31]. However, it might theoretically have a large range of possible values between 4 eV and 30 eV as found in graphite and carbon nanotube materials [43]. The value of μ_c is directly obtained by substituting equation (2) into equation (3).

The Zs_{ON} value is found by increasing the charge carrier density n until saturation is reached as LA

TABLE II: Selected surface impedance Zs values

Set	1		2	
State	ON	OFF	ON	OFF
n [m^{-2}]	$5{\cdot}10^{17}$	$6{\cdot}10^{14}$	$5{\cdot}10^{17}$	$6{\cdot}10^{14}$
V_b [V]	22.72	$\sim$0	22.72	$\sim$0
μ_L [m^2/Vs]	2.7		2.7	
D [eV]	4		18	
T [K]	295		295	
Zs [$\Omega/\square$]	6 + j0.3	2580 + j6	34 + j0.3	2580 + j6

phonon scattering becomes dominant and at the same time the voltage V_b is not too high (22.7 V). On the other hand, the value for Zs_{OFF} is obtained by setting the minimum achievable chemical potential equal to the energy of the electron-hole puddles ($\mu_{c,min} = \zeta_{puddle}$) - equation (5). The carrier inhomogeneity density $\tilde{n}$=6$\times 10^{14}$ m^{-2} is obtained from [34]. The value of μ_L is also extracted from reference [34]. V_b values are calculated using equation (3) by considering selected values of ϵ and d in Table I, and n values in Table II. Although the resulting V_b values might be too large for implementation in low voltage devices, e.g. mobile phones, the values can be reduced in the future by using thinner dielectrics with higher relative permittivity or ion-gels once the technology is available. For example, in [44] the authors used ion-gel substrates to achieve large changes in the charge carrier density - between $n \approx 3\times 10^{16}\ m^{-2}$ and $n \approx 2.65\times 10^{17}\ m^{-2}$ - by only applying a difference in voltage bias V_b of 1.53 V thanks to the high capacitance density of the ion-gel. Likewise, in [45] the authors achieved charge carrier densities of up to $n \approx 1\times 10^{18}\ m^{-2}$ for voltage bias values of only 5 V. The charge carrier density values obtained in [44], [45] are very similar to the ones needed in this paper, and hence, with ion-gel substrate, the required voltage bias values could be substantially reduced. However, ion-gels have not been considered in this paper because currently very low values of carrier mobility $\mu_L \approx$0.0075 - 0.08 m^2/Vs have been obtained [44]–[48]. For the OFF state, the resulting V_b values are near 0 V due to having very low inhomogeneity density $\tilde{n}$.

Finally, for all the scenarios evaluated in Section V the antenna substrate selected is Polystyrene (PS) with ϵ_r=2.4 and tanδ=0.0002 [49]. The antenna substrate thickness (H) is set to 2.1 mm as the space available in mobile devices is very limited. In the next section, the proposed antenna designs are simulated and analysed.

V. RESULTS

The results here are obtained from the transient solver (time domain solver) in the CST Microwave Studio 2015. The graphene sheets have been defined as solid sheets with thickness equal to zero and simulated as ohmic sheet surface impedances. The excitation is a discrete port with 50 Ω port impedance. The efficiencies calculated from CST follow equation (14);

$$\eta_t = \left(\frac{P_{rad}}{P_{sim}}\right) \times 100 \tag{14}$$

where η_t is the total antenna efficiency (%), P_{rad} is the power being radiated by the antenna (W) and P_{sim}=0.5 W is the power generated by the excitation signal.

TABLE III: Set up parameters for WIFI scenario, see Fig. 2a

$Lmain$ [mm]	W [mm]	$Lleft$ [mm]	$Lright$ [mm]	X [mm]	Y [mm]
23	14.7	5	7.3	5.5	2

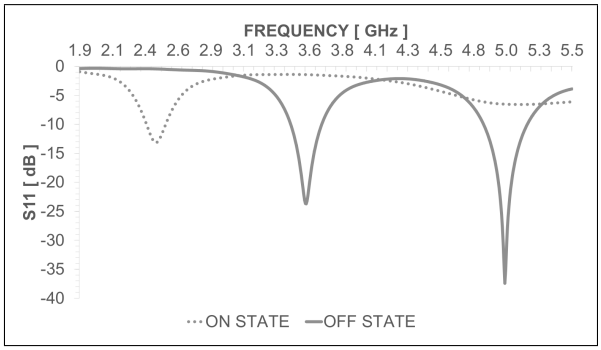

Fig. 3: Reflection coefficient for the WIFI design with the extensions activated (dotted line) and with the extensions deactivated (solid line).

A. WIFI SCENARIO

The following scenario evaluates the first design to cover three bands in WIFI (2.4 GHz, 3.6 GHz and 5 GHz), see Fig. 2a. The extensions are activated and deactivated to change the resonant frequencies between 2.4 GHz and 3.6 GHz. In this scenario, the TM_{110} mode is used as the antenna is fed in a corner which allows an extra resonance at 5 GHz by adjusting the width of the main patch W. See Table III for the antenna dimensions.

Fig. 3 provides the reflection coefficient ($S11$) parameters for the WIFI scenario. When the extensions are deactivated (OFF state), the resonant frequencies are found at 3.6 GHz and 5 GHz. On the other hand, when the extensions are activated (ON state), the lower resonant frequency changes from 3.6 GHz to 2.4 GHz. Thus the activation and deactivation of the extensions is required to switch between these two resonant frequencies.

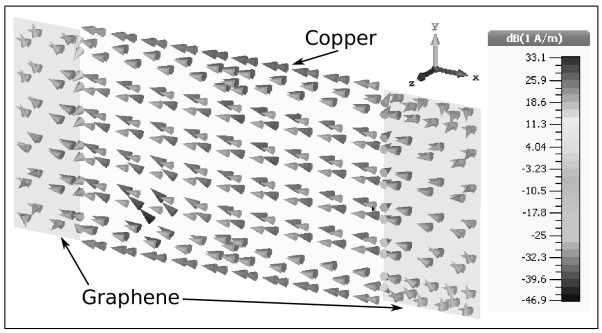

(a)

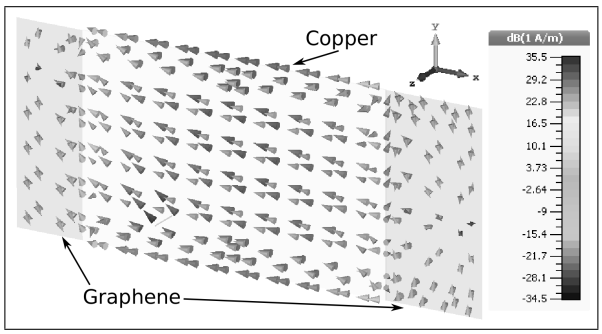

(b)

Fig. 4: Surface current density on the WIFI antenna at (a) 2.4 GHz and (b) 3.6 GHz.

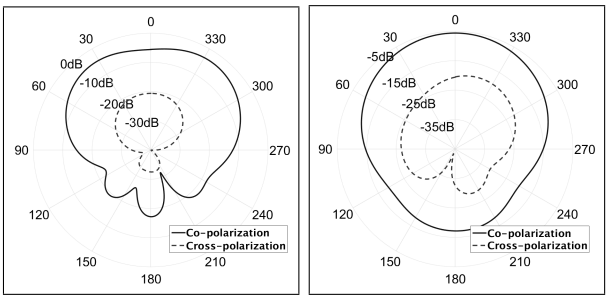

(a) E Plane (x-z plane)

(b) H plane (y-z plane)

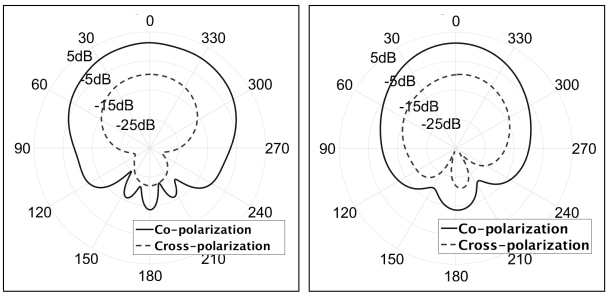

(c) E Plane (x-z plane)

(d) H plane (y-z plane)

Fig. 5: Radiation patterns of the WIFI antenna at (a)-(b) 2.4 GHz and (c)-(d) 3.6 GHz.

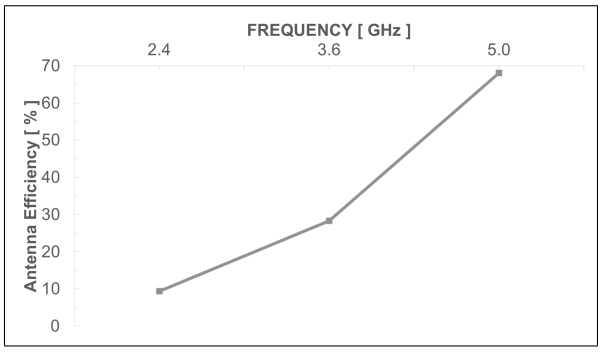

Fig. 6: Antenna efficiencies of the WIFI design.

In order to confirm that the activation/deactivation of the graphene extensions do change the antenna behaviour, Fig. 4 provides the surface current distribution along the main patch and the graphene extensions for frequencies 2.4 GHz and 3.6 GHz, when the graphene extensions are either activated or deactivated respectively. As expected, when the graphene extensions are on the OFF state - at 3.6 GHz, little current is allowed to propagate along the extensions. In contrast, when the graphene extensions are in the ON state - at 2.4 GHz, substantially more current is able to propagate along the extensions and contribute to the electromagnetic radiation. This effectively changes the resonant length of the antenna and hence its resonant frequency.

Fig. 5 shows the radiation patterns at 2.4 GHz and 3.6 GHz, when the graphene extensions are activated and deactivated respectively. As observed, all the radiation patterns are similar in shape and close to the characteristics for a typical square patch antenna, showing that the graphene extensions have little effect on the shape of the radiation pattern. The results for the surface current and radiation pattern at 5 GHz are not included here, however, the same conclusions apply at that frequency. The obtained antenna gains are -3.4 dB, 1.3 dB and 5.2 dB at 2.4 GHz, 3.6 GHz and 5 GHz respectively.

The antenna efficiencies extracted from the WIFI design are summarized in Fig. 6. The antenna efficiencies η_t show that when the antenna radiates at 2.6 GHz, η_t is lower than at any of the other two frequencies because of the graphene extensions attenuating the currents that contribute to radiation at that frequency. The power lost on graphene is about 337 mW which is a 67% of the total loss. When the graphene extensions are deactivated, in theory, the presence of the graphene extensions should affect equally at 3.6 GHz and 5 GHz, but their respective antenna efficiencies are not the same. An explanation

might be that at 3.6 GHz, the graphene sheet must stop as much as possible any current propagating to the extensions. The better the graphene extensions achieve that, the less power is lost in graphene and the more is radiated. On the contrary, at 5 GHz whether currents are attenuated or not does not strongly affect the antenna efficiency but the antenna matching at that frequency, see Fig. 3. In general, it is demonstrated that the WIFI design proposed here is able to cover the target bands but the antenna efficiency at 2.4 GHz might be too low.

To demonstrate the impact of the surface impedance on the ON state (2.4 GHz), the same antenna is evaluated but now Zs_{ON}=6+j0.3 $\Omega/\square$ (set 1 in Table II) instead of Zs_{ON}=34+j0.3 $\Omega/\square$ (set 2 in Table II) by assuming that the deformation potential D is improved from D=18 eV to D=4 eV. The resulting value of η_t changes from 9.4% to 35.5% as the the power lost in graphene has been reduced from 337 mW to 253 mW at 2.4 GHz. This shows how important is to reduce the graphene surface impedance for the ON state Zs_{ON} in order to have reasonable antenna efficiencies. Unfortunately, the lower limit of Zs_{ON} depends on the deformation potential D which is yet not fully determined from experimental studies, and consequently, variations when defining this parameter strongly affects the final performance. Alternatively, a similar improvement would be achieved if the charge carrier mobility μ_L is increased by improving the fabrication, the transfer process and the use of even better dielectrics which graphene can be deposited on. In that case, both surface impedances, Zs_{ON} and Zs_{OFF}, would decrease. However, reducing the OFF state surface impedance would cause a lower antenna efficiency in the OFF state, which highlights the importance of achieving a high ratio difference between the surface impedances of the ON and OFF states.

1) TUNABLE BANDWIDTH AND ANTENNA MATCHING: Here, the antenna matching and operational bandwidth is studied when different surface resistances Rs are selected. Note that by changing the Rs, the surface reactance Xs of the surface impedance - $Zs = Rs + jXs$ - is also slightly changed but has no impact on the final result. As observed in Fig. 7, this allows to improve the antenna matching and tune the operational bandwidth BW. For instance, at 2.4 GHz, the value of the reflection coefficient goes from -8.7 dB to -13.2 dB by just selecting Rs=51 $\Omega/\square$ or Rs=31 $\Omega/\square$ respectively, see Fig. 8. This effect is also reproduced for the 3.6 GHz and 5 GHz frequencies. The operational bandwidth can be tuned from a maximum all the way down to 0 MHz, which means not having the condition $S11 \leq$10 dB, by again selecting a proper Rs. This might help to

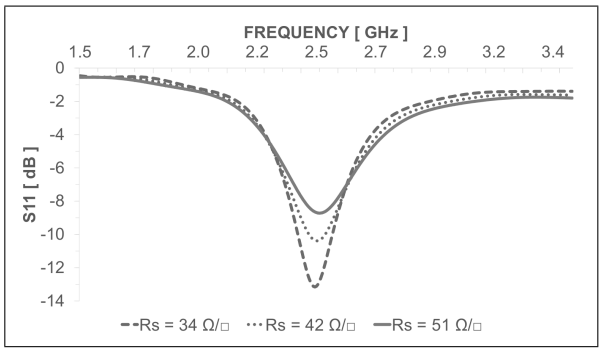

(a)

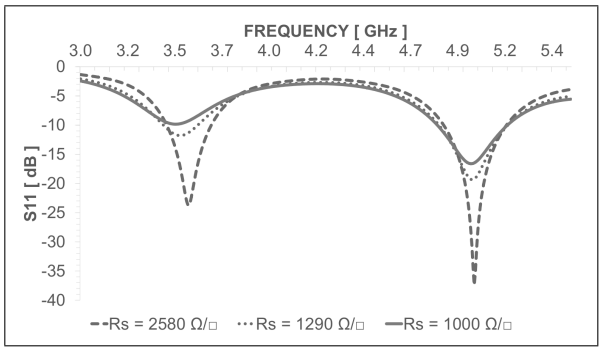

(b)

Fig. 7: Reflection coefficient for the WIFI antenna with variable BW for the (a) ON state and (b) OFF state.

reduce the complexity of the antenna matching network in future reconfigurable antennas made partially of graphene. The resulting antenna efficiencies are close to each other, however, the best efficiencies are again found when both Rs_{ON} and Rs_{OFF} are minimum and maximum respectively.

2) TUNABLE RESONANT FREQUENCY: Since intermediate values of the graphene surface impedance between Zs_{ON} and Zs_{OFF} can be selected, it is theoretically possible to select any resonant frequency between the two edge frequencies limited by these values. To show an example of this, Fig. 9 shows the reflection coefficient of the WIFI antenna design, Fig. 2a, for four different values of Rs. Both extension lengths have been shrunk to L_{left}=L_{right}=3 mm to keep a good matching of the antenna over the range of operating frequencies. In this case, the four different values of Rs provide four different resonant frequencies, see Fig. 10. Interestingly, the antenna efficiency η_t for the two extreme values Rs=70 $\Omega/\square$ and Rs=2580 $\Omega/\square$ are now better than the ones obtained in the WIFI scenario for Rs_{ON}=34 $\Omega/\square$ and Rs_{OFF}=2580 $\Omega/\square$, see section V-A. Clearly, shorter graphene extensions cause less ohmic losses

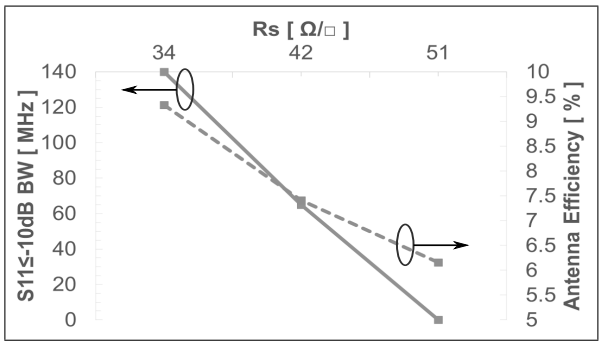

(a)

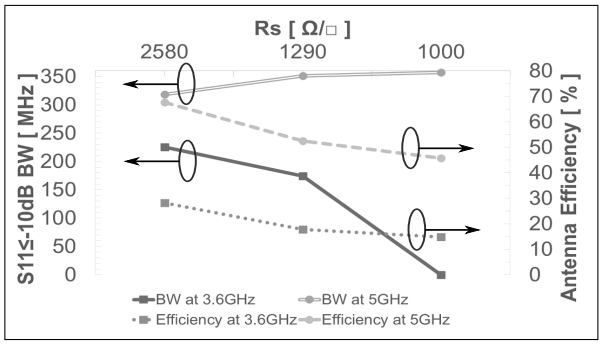

(b)

Fig. 8: Bandwidth and antenna efficiency variation for different values of Rs at a) 2.4 GHz and b) 3.6 GHz and 5 GHz.

but smaller changes in the resonant frequencies since now the lower resonant frequency is 3 GHz instead of 2.4 GHz. For the intermediate resonant frequencies, the antenna efficiencies are worse compared to the two edge frequencies. The cause is that as more and more current is allowed to propagate to the extensions (by reducing the Rs), the current is being substantially attenuated due to large values of Rs. The ability to select any resonant frequency within a specific range might prove very useful in wearable applications, where streching and bending affects the resonant frequency of the antenna among other parameters.

B. LTE SCENARIO

The second design, Fig. 2b, covers four bands of LTE (1.8 GHz, 2.1 GHz, 2.6 GHz and 3.6 GHz) by switching ON and OFF different graphene strips. This scenario also uses the TM_{110} mode for radiating. The values of Zs_{ON} and Zs_{OFF} are assigned from the Set 2 in Table II. See Table IV for the structure dimensions.

Fig. 11 provides the $S11$ parameters for the LTE scenario. When all four graphene strips are activated,

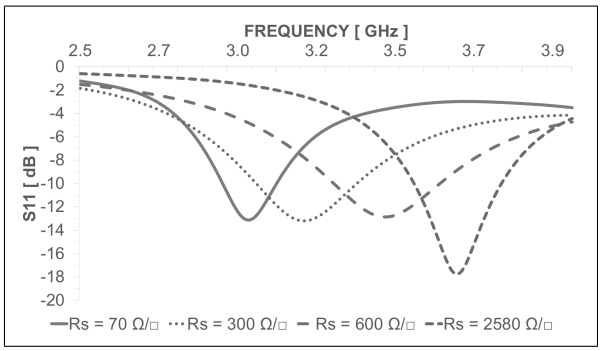

Fig. 9: Reflection coefficient for the WIFI design with intermediate Rs values selected.

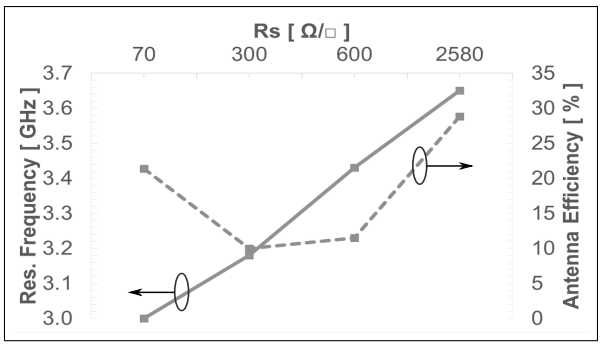

Fig. 10: Resonant frequency and antenna efficiency variation as Rs changes.

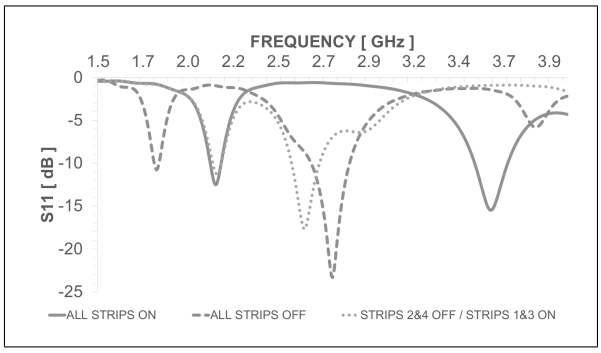

Fig. 11: Reflection coefficient for the LTE design with all strips activated (solid line), all strips deactivated (dashed line), and with strips 2 and 4 deactivated and strips 1 and 3 activated (dotted line).

the antenna operates efficiently at 2.1 GHz and 3.6 GHz. Conversely, when all four strips are deactivated, the antenna switches now to 1.8 GHz operation. Finally, when strips 2 and 4 are OFF and strips 1 and 3 are ON, the antenna achieves good matching at 2.6 GHz. Ideally, the antenna should switch between the four

TABLE IV: Set up parameters for LTE scenario, see Fig. 2b

$Lmain$ [mm]	W [mm]	$L1$ [mm]	$W1$ [mm]	$L2$ [mm]	$W2$ [mm]	$L3$ [mm]	$W3$ [mm]	$L4$ [mm]	$W4$ [mm]	$D1$ [mm]	$D2$ [mm]	X [mm]	Y [mm]
39	22	2	8.5	11	2	2	8.5	11	2	23.5	10	12.5	1

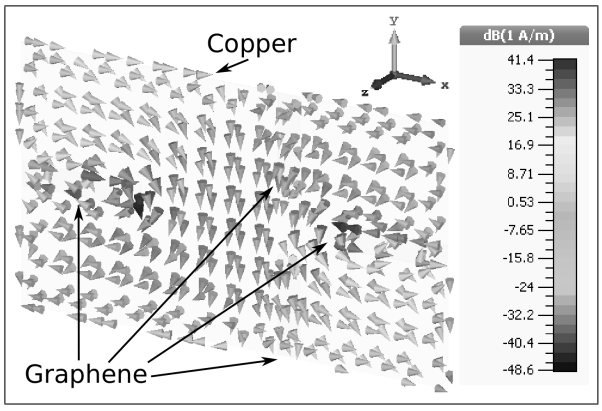

(a)

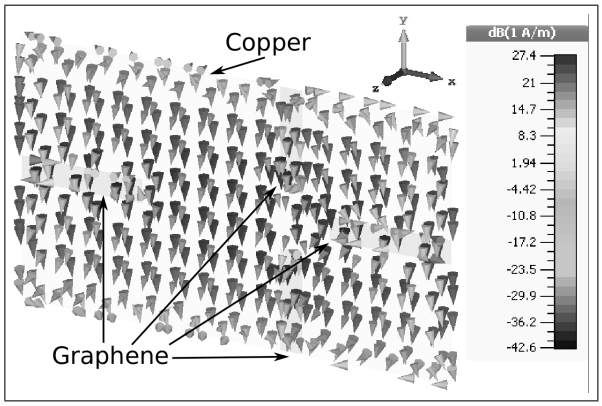

(b)

Fig. 12: Surface current density in the LTE antenna at (a) 2.6 GHz and (b) 3.6 GHz.

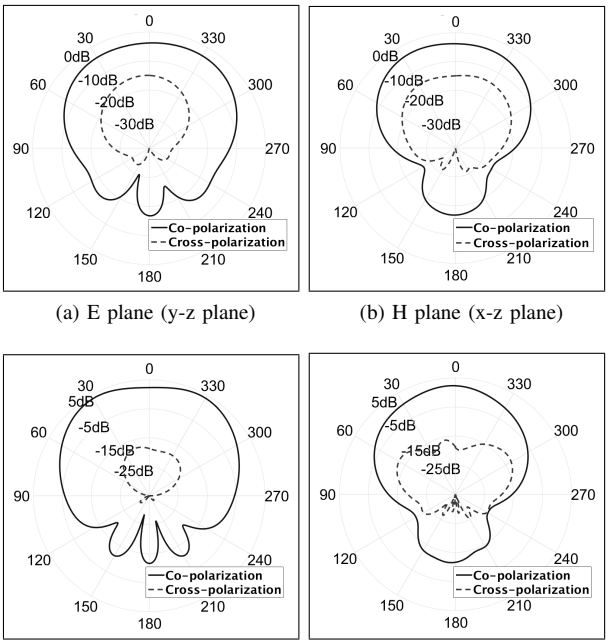

(a) E plane (y-z plane)

(b) H plane (x-z plane)

(c) E plane (y-z plane)

(d) H plane (x-z plane)

Fig. 13: Radiation patterns of the LTE antenna at (a)-(b) 2.6 GHz and (c)-(d) 3.6 GHz.

desired bands by switching ON or OFF all four strips at the same time. Unfortunately, when the four strips are deactivated the secondary frequency is found to be slightly over 2.6 GHz. This is because deactivating strips 1 and 3 affects the resonance at 2.6 GHz.

The surface current densities have been simulated to show the effect of the graphene strips on the behaviour of the antenna. Fig. 12 shows the current distributions along the main patch and the graphene strips at 2.6 GHz and 3.6 GHz, where graphene strips 2 and 4 (Fig. 2b) are activated and deactivated. When the graphene strips are set to the ON state, Fig. 12b, the current is allowed to propagate through the strips. However, when the graphene strips are set to the OFF state, Fig. 12a, the currents are not allowed to propagate through the strips but are diverted around them. That makes the currents travel longer paths and therefore the antenna resonance is found at a lower frequency. Similar behaviour is found at 1.8 GHz and 2.1 GHz.

Fig. 13 shows the radiation patterns at 2.6 GHz and 3.6 GHz, where again graphene strips 2 and 4 are activated and deactivated. The resulting radiation patterns are again similar in shape and close to a typical square patch antenna, as previously observed in the WIFI scenario. Thus, the addition of the graphene strips seems to not strongly affect the shape of the radiation pattern. The radiation patterns for the remaining resonant frequencies, 1.8 GHz and 2.1 GHz, are very similar to the ones at 2.6 GHz and 3.6 GHz and therefore are not shown here. The resulting antenna gains are -1.6 dB, -0.7 dB, -3.3 dB and 3.9 dB at 1.8 GHz, 2.1 GHz, 2.6 GHz and 3.6 GHz respectively.

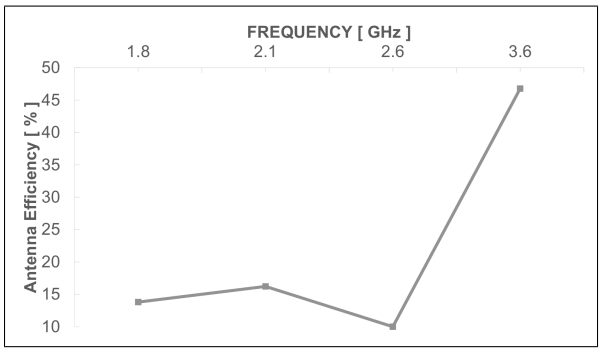

Fig. 14: Antenna efficiencies of the LTE design.

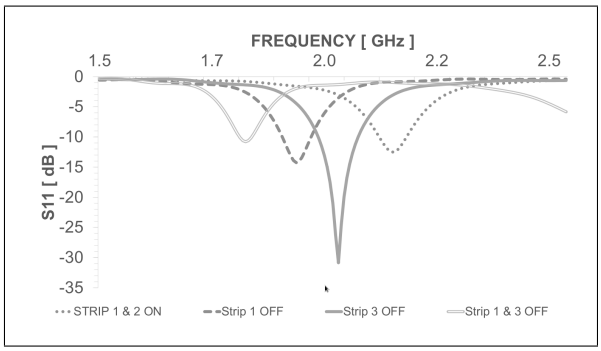

Fig. 15: Reflection coefficient for the LTE design with strips 1 and 3 activated (dotted line), strip 1 deactivated and strip 3 activated (dashed line), strip 2 deactivated and 1 activated (solid line) and strip 1 and 3 deactivated (double solid line).

The efficiency results obtained are shown in Fig. 14. The worst efficiency is found at 2.6 GHz due to a large change of frequency being forced - from 3.6 GHz to 2.6 GHz.

1) INDIVIDUAL GRAPHENE STRIP SWITCHING: In the LTE design, in order to change the resonant frequencies, pairs of strips are accordingly switched ON and OFF. However, it could be possible to individually activated or deactivate any of strips independently and hence achieve intermediate resonant frequencies. Fig. 15 presents the results for individually switching graphene strips 1 and 3, where the widths of strips 1 and 3 were changed from $W1$=$W3$=8.5 mm to $W1$=9.5 mm and $W3$=7.5 mm. As shown, if both graphene strips are on the ON state, the antenna is radiating at 2.1 GHz, as in the previous LTE configuration. But, if strip 1 is now individually changed to the OFF state while strip 3 is kept on the ON state, the resonance changes to 1.92 GHz. On the contrary, if strip 3 is the one changed to the OFF state and the strip 1 is kept on the ON state, the obtained resonant frequency is now 2.01 GHz. Finally, if both are switched to the OFF state, then the antenna resonates to 1.8 GHz as in the previous scenario. The efficiencies for the two extra resonant frequencies achieved here - 1.92 GHz and 2.01 GHz - are found to be 11% and 15.5% respectively, in the same order as for 1.8 GHz. Therefore, frequency reconfigurable antennas made partially of graphene extensions/strips could provide as many resonant frequencies as combinations of activating/deactivating graphene sheets without causing a drop in the the antenna efficiency.

C. PERFORMANCE COMPARISON

Here, the results obtained from the proposed WIFI and LTE antennas are compared to some other planar frequency reconfigurable antennas found in the literature. In [2], an anular slot antenna is configured to switch between two operating frequencies by integrating MEMS. In [6], a planar inverted-F antenna (PIFA) covers some commercial mobile phone bands by implementing multiple PIN-diodes. In [8], a patch antenna with a varactor loaded slot can operate at any frequency within a specific range by applying different DC voltages. Table V summarizes the comparison.

As observed from Table V, the antenna efficiencies obtained when using graphene are lower compared to any of the other switching technologies in the low and high limits. This is expected as graphene is still a material under development. On the other hand, the voltage required to switch between ON and OFF states in graphene is within the values required for the other switching technologies to switch between states. Moreover, the negligible static power drained by graphene is the lowest of all. However, when graphene is switched between the ON and OFF states, there is a short burst of peak power consumed in the bias circuit. This is explained in more detail in Section V-D. Note that no data was found for MEMS used in [2]. However, MEMS switches can provide very low power consumption similar to graphene [10].

Graphene is used here as part of the radiating structure which does not add extra weight or space. However, in the other papers, the RF switches are elements added to the structure that do not contribute to radiation and increase the weight and volume of the antenna. As shown in this section, implementing graphene in antennas can provide the ON/OFF behaviour similar to MEMS and PIN-diode switches. In addition, it provides the continous frequency selection found in antennas loaded with varactors with the extra feature of bandwidth selection. Therefore, using graphene converges multiple

TABLE V: Comparison of different reconfigurable antennas

Reference	Technology	Frequencies Covered	Antenna Efficiency	Voltage bias	Power drain
This work WIFI design	Graphene	2.4GHz, 3.6GHz and 5GHz	9.4%(D=18eV) 35%(D=4eV) to 68%	22.7V	0W
This work LTE design	Graphene	1.8GHz, 2.1GHz, 2.6GHz and 3.6GHz	10% to 46.8%	22.7V	0W
[2]	MEMS	2.4GHz and 5.2GHz	90% to 92%	20V	-
[6]	PIN-diode	0.7GHz, 0.85/0.9GHz, 1.8/1.9GHz and 2.3/2.5GHz	52.1% to 85.4%	0.75V	2.25mW
[8]	Varactor	continuous from 3.24GHz to 4.35GHz	38% to 90%	30V	250mW

modes of operation into a single solution. Additionally, substituting some metallic parts of the structure with graphene would allow for reconfigurable antennas where transparency and/or flexibility is desired. The remaining metallic part would also require to be a transparent and/or flexible low resistive conductor such as transparent thin films, eTextiles or conductive inks. Finally, graphene can easily operate at mm-wave and THz regime [14]–[21], [24] where conventional switches will perform poorly or even not work at all. For instance, realistic cutoff frequencies (figure-of-merit/10) for FET-based, PIN-diode/varactors and MEMS are around 40GHz, 190GHz and 900GHz respectively [10].

TABLE VI: P_{peak} values for WIFI based designs

WIFI (Section V-A)	n [m^{-2}]	A [mm^2]	P_{peak} [mW]
Zs_{ON}= 34+j0.3 [$\Omega/\square$]	$5{\cdot}10^{17}$	180.8	330.6
Zs_{ON}= 6+j0.3 [$\Omega/\square$]	$5{\cdot}10^{17}$	180.8	330.6
Tunable BW and $S11$ (Section V-A1)	n [m^{-2}]	A [mm^2]	P_{peak} [mW]
Rs_{ON}= 34 [$\Omega/\square$]	$5{\cdot}10^{17}$	180.8	330.6
Rs_{ON}= 42 [$\Omega/\square$]	$1.8{\cdot}10^{17}$	180.8	42.8
Rs_{ON}= 51 [$\Omega/\square$]	$1.05{\cdot}10^{17}$	180.8	14.6
Tunable $f_{resonant}$ (section V-A2)	n [m^{-2}]	A [mm^2]	P_{peak} [mW]
Rs_{ON}= 70 [$\Omega/\square$]	$5.7{\cdot}10^{16}$	88.2	2.1
Rs_{ON}= 300 [$\Omega/\square$]	$8.5{\cdot}10^{15}$	88.2	0.0466
Rs_{ON}= 600 [$\Omega/\square$]	$3.9{\cdot}10^{15}$	88.2	0.0098

D. SWITCHING POWER CONSUMPTION

Table VI and VII provide the peak power consumed (P_{peak}) for all the scenarios evaluated in this paper when switching from one operating frequency to another due to the change of required values of charge carrier density n. For example, when switching between 2.4 GHz and 3.6 GHz in the WIFI design as the graphene extensions are activated or deactivated respectively. It is important to highlight here that the power consumption happens during a very short period of time - t $\ll$ switching time - and quickly drops to zero. So in normal use, hybrid metal-graphene reconfigurable antennas have very low power consumption. The total power shown is calculated by using equation (10) where the dielectric thickness d, the relative permittivity ϵ and the time constant τ_{RC} are set using the values in Table I. Specific values such as the charge carrier density n and the physical area of graphene A are extracted from Tables II, III and IV. Note that, in the evaluated scenarios there are from two to four graphene sheets being fed and the total power consumed is the addition of the power consumed by each individual sheet as it switches ON or OFF.

From Table VI and VII it is observed that the peak power consumption substantially decreases as the physical dimensions of the graphene sheets reduce. For example, when the area of the extensions of the WIFI design is reduced from 180.8 mm^2 to 88.2 mm^2, or when only strips 1 and 3 are turned ON - total area of 34 mm^2 - instead of all the strips ON - total area 78 mm^2 - in the LTE design, the value of P_{peak} is reduced. This is another reason for implementing graphene in hybrid metal-graphene antennas instead of full graphene antennas. Likewise, low values of charge carrier density n also help to reduce the power consumed. Interesting results are obtained for the tunable resonant frequency scenario in Table VI (Subsection V-A2) where very low peak power consumptions are obtained - 2.1 mW, 46.6 μW and 9.8 μW - for changes in the resonant frequency of up to 650 MHz. Likewise, relaxing the values for the ON state surface impedance (Zs_{ON}) seems to be also beneficial on the point of view of power consumption. For example, in the tunable bandwidth and matching scenario, selecting the Rs_{ON}=51 $\Omega/\square$ instead of Rs_{ON}=34 $\Omega/\square$ reduces the neccessary carrier density significantly and hence the peak power consumption drops by more than 20 times, from 330.6 mW to 14.6 mW.

It is also worth to analyse the impact of the deformation potential D value in the power consumption. As seen in the WIFI section, see section V-A, the antenna efficiency can be greatly improved by assuming Zs_{ON}=6+j0.3 $\Omega/\square$ due to a much better achievable deformation potential D=4 eV. However, if instead of dropping the value of Zs so much, it is enough to have Zs_{ON}=34+j0.3 (assuming that the antenna efficiency

TABLE VII: P_{peak} values for LTE based designs

LTE scenario (V-B)	n [m^{-2}]	A [mm^2]	P_{peak} [mW]
All Zs_{ON}= 34+j0.3 [$\Omega/\square$]	$5{\cdot}10^{17}$	78	142.6
Strips 1-3 Zs_{ON}= 34+j0.3 [$\Omega/\square$]	$5{\cdot}10^{17}$	34	62.2
Individual Strip V-B1)	n [m^{-2}]	A [mm^2]	P_{peak} [mW]
Strip 1 Zs_{ON}= 34+j0.3 [$\Omega/\square$]	$5{\cdot}10^{17}$	19	34.7
Strip 3 Zs_{ON}= 34+j0.3 [$\Omega/\square$]	$5{\cdot}10^{17}$	15	27.4

obtained is acceptable), then, the required charge carrier density n to achieve that value would be n=7$\times10^{16}$ m^{-2} instead of n=5$\times10^{17}$ m^{-2} (an order of magnitude lower). This reduction in the n would cause a reduction of the peak power consumption from 330.6 mW to just 6.6 mW, a factor of 50 times less. As a result, there is a trade off between in one hand a required antenna performance, such as achievable frequency reconfigurability and/or antenna efficiency; and on the other hand, the allowed switching power consumption. It is possible to greatly improve one aspect at the expense of increasing the other.

VI. CONCLUSIONS

This paper has analysed the performance of using graphene in frequency reconfigurable antennas in the microwave regime via the simulation of two hybrid metal-graphene antennas for WIFI and LTE applications. Implementing graphene as a material with tunable surface impedance allowed large frequency reconfigurability - up to 1.2 GHz change - with additional tunability of the antenna matching - up to 20 dB improvement - and bandwidth - up to 225 MHz increase. Although very low power consumption is achieved during normal operation, moderate values of the instantaneous peak power ($\leq$ 330.6 mW) are present during the switching process which only occurs during very short time periods ($\leq$ 1.6 ms). The proposed antennas can achieve high reconfigurability degree in terms of changing operational frequency but at the expense of lower antenna efficiencies - between 9.4% and 68%. To mitigate this effect, the losses due to the presence of graphene must be reduced while still keeping the necessary reconfigurability. This might drive to study other types of antennas where small graphene sheets can be integrated without compromising the antenna performance. To ultimately confirm the feasibility of the proposed designs, prototypes should be built and measured. Its physical study will include effects not considered in this paper such as the contact resistance, the possible parasitic effects of the DC bias circuit (if needed) and the impact of adding the electric field effect structure between the radiating patch and the ground.

REFERENCES

[1] C. W. Jung, M. J. Lee, G. P. Li, and F. De Flaviis, "Reconfigurable scan-beam single-arm spiral antenna integrated with RF-MEMS switches," *IEEE Trans. Antennas Propag.*, vol. 54, no. 2, pp. 455–463, 2006.

[2] B. A. Cetiner, G. R. Crusats, L. Jofre, and N. Biyikli, "Rf mems integrated frequency reconfigurable annular slot antenna," *IEEE Trans. Antennas Propag.*, vol. 58, no. 3, pp. 626–632, March 2010.

[3] L. N. Pringle *et al.*, "A reconfigurable aperture antenna based on switched links between electrically small metallic patches," *IEEE Trans. Antennas Propag.*, vol. 52, no. 6, pp. 1434–1445, 2004.

[4] T. Aboufoul, A. Alomainy, and C. Parini, "Reconfiguring UWB monopole antenna for cognitive radio applications using GaAs FET switches," *IEEE Antennas Wireless Propag. Lett*, vol. 11, pp. 392–394, 2012.

[5] D. Peroulis, K. Sarabandi, and L. P. B. Katehi, "Design of reconfigurable slot antennas," *IEEE Trans. Antennas Propag.*, vol. 53, no. 2, pp. 645–654, 2005.

[6] S. W. Lee and Y. Sung, "Compact frequency reconfigurable antenna for lte/wwan mobile handset applications," *IEEE Trans. Antennas Propag.*, vol. 63, no. 10, pp. 4572–4577, Oct 2015.

[7] C. R. White and G. M. Rebeiz, "Single-and dual-polarized tunable slot-ring antennas," *IEEE Trans. Antennas Propag.*, vol. 57, no. 1, pp. 19–26, 2009.

[8] A. Khidre, F. Yang, and A. Z. Elsherbeni, "A patch antenna with a varactor-loaded slot for reconfigurable dual-band operation," *IEEE Trans. Antennas Propag.*, vol. 63, no. 2, pp. 755–760, 2015.

[9] R. L. Haupt, "Reconfigurable patch with switchable conductive edges," *Microw. Opt. Technol. Lett.*, vol. 51, no. 7, pp. 1757–1760, 2009.

[10] R. L. Haupt and M. Lanagan, "Reconfigurable antennas," *IEEE Antennas Propag. Mag*, vol. 55, no. 1, pp. 49–61, 2013.

[11] A. H. N. Castro, F. Guinea, N. M. R. Peres, K. Novoselov, and A. Geim, "The electronic properties of graphene," *Rev. Mod. Phys.*, vol. 81, pp. 109–162, Jan 2009.

[12] F. Bonaccorso, Z. Sun, T. Hasan, and A. C. Ferrari, "Graphene photonics and optoelectronics," *Nature Photon.*, vol. 4, no. 9, pp. 611–622, 2010.

[13] C. Lee, X. Wei, J. W. Kysar, and J. Hone, "Measurement of the elastic properties and intrinsic strength of monolayer graphene," *Science*, vol. 321, no. 5887, pp. 385–388, 2008.

[14] M. Dragoman, A. A. Muller, D. Dragoman, F. Coccetti, and R. Plana, "Terahertz antenna based on graphene," *J. Appl. Phys.*, vol. 107, no. 10, p. 104313, 2010.

[15] J. S. Gomez-Diaz and J. Perruisseau-Carrier, "Microwave to THz properties of graphene and potential antenna applications," in *2012 Int. Symp. on Antennas and Propagation (ISAP)*. IEEE, 2012, pp. 239–242.

[16] M. Tamagnone, J. S. Gomez-Diaz, J. R. Mosig, and J. Perruisseau-Carrier, "Analysis and design of terahertz antennas based on plasmonic resonant graphene sheets," *J. Appl. Phys.*, vol. 112, no. 11, p. 114915, 2012.

[17] M. Tamagnone, J. Gomez-Diaz, J. R. Mosig, and J. Perruisseau-Carrier, "Reconfigurable terahertz plasmonic antenna concept using a graphene stack," *Appl. Phys. Lett.*, vol. 101, no. 21, p. 214102, 2012.

[18] Y. Yao, M. A. Kats, P. Genevet, N. Yu, Y. Song, J. Kong, and F. Capasso, "Broad electrical tuning of graphene-loaded plasmonic antennas," *Nano Lett.*, vol. 13, no. 3, pp. 1257–1264, 2013.

[19] J. M. Jornet and I. F. Akyildiz, "Graphene-based plasmonic nano-antenna for terahertz band communication in nanonetworks," *IEEE J. Sel. Areas Commun*, vol. 31, no. 12, pp. 685–694, December 2013.
[20] M. Esquius-Morote, J. S. Gmez-Daz, and J. Perruisseau-Carrier, "Sinusoidally modulated graphene leaky-wave antenna for electronic beamscanning at thz," *IEEE Trans. THz Sci. Technol.*, vol. 4, no. 1, pp. 116–122, Jan 2014.
[21] E. Carrasco, M. Tamagnone, J. R. Mosig, T. Low, and J. Perruisseau-Carrier, "Gate-controlled mid-infrared light bending with aperiodic graphene nanoribbons array," *Nanotechnology*, vol. 26, no. 13, p. 134002, 2015.
[22] X. Huang *et al.*, "Highly flexible and conductive printed graphene for wireless wearable communications applications," *Scientific reports*, vol. 5, 2015.
[23] J. Perruisseau-Carrier, M. Tamagnone, J. S. Gomez-Diaz, and E. Carrasco, "Graphene antennas: Can integration and reconfigurability compensate for the loss?" in *2013 European Microwave Conf. (EuMC)*, Oct 2013, pp. 369–372.
[24] M. Tamagnone, J. S. G. Diaz, J. Mosig, and J. Perruisseau-Carrier, "Hybrid graphene-metal reconfigurable terahertz antenna," in *2013 IEEE MTT-S Int. Microwave Symp. Dig. (IMS)*, June 2013, pp. 1–3.
[25] S. Bae *et al.*, "Roll-to-roll production of 30-inch graphene films for transparent electrodes," *Nat. Nanotechnol.*, vol. 5, no. 8, pp. 574–578, 2010.
[26] C. N. Alvarez, R. Cheung, and J. S. Thompson, "Graphene reconfigurable antennas for LTE and WIFI systems," in *2014 Antennas and Propagation Conf. (LAPC 2014)*, Nov 2014, pp. 434–438.
[27] V. P. Gusynin, S. G. Sharapov, and J. P. Carbotte, "Magneto-optical conductivity in graphene," *J. Phys.: Condens. Matter*, vol. 19, no. 2, p. 026222, 2007.
[28] G. W. Hanson, "Dyadic Greens functions and guided surface waves for a surface conductivity model of graphene," *J. Appl. Phys.*, vol. 103, no. 6, 2008.
[29] N. M. R. Peres, "*Colloquium* : The transport properties of graphene: An introduction," *Rev. Mod. Phys.*, vol. 82, pp. 2673–2700, Sep 2010.
[30] K. S. Novoselov *et al.*, "Electric field effect in atomically thin carbon films," *Science*, vol. 306, no. 5696, pp. 666–669, 2004.
[31] J. H. Chen, C. Jang, S. Xiao, M. Ishigami, and M. S. Fuhrer, "Intrinsic and extrinsic performance limits of graphene devices on SiO_2," *Nat. Nanotechnol.*, vol. 3, no. 4, pp. 206–209, 2008.
[32] J. Martin *et al.*, "Observation of electron–hole puddles in graphene using a scanning single-electron transistor," *Nature Phys.*, vol. 4, no. 2, pp. 144–148, 2008.
[33] K. I. Bolotin *et al.*, "Ultrahigh electron mobility in suspended graphene," *Solid State Commun.*, vol. 146, no. 9, pp. 351–355, 2008.
[34] N. Petrone *et al.*, "Chemical vapor deposition-derived graphene with electrical performance of exfoliated graphene," *Nano Lett.*, vol. 12, no. 6, pp. 2751–2756, 2012, pMID: 22582828.
[35] M. Roschke and F. Schwierz, "Electron mobility models for 4H, 6H, and 3C SiC [MESFETs]," *IEEE Trans. Electron Devices*, vol. 48, no. 7, pp. 1442–1447, Jul 2001.
[36] R. A. Street, J. Kakalios, and M. Hack, "Electron drift mobility in doped amorphous silicon," *Phys. Rev. B*, vol. 38, pp. 5603–5609, Sep 1988.
[37] J. Gomez-Diaz, C. Moldovan, S. Capdevila, J. Romeu, L. Bernard, A. Magrez, A. Ionescu, and J. Perruisseau-Carrier, "Self-biased reconfigurable graphene stacks for terahertz plasmonics," *Nat. Commun.*, vol. 6, 2015.
[38] ITUR, "M. 2134. requirements related to technical performance for imt-advanced radio interface (s)," Technical Report, 3GPP, Tech. Rep., 2008.
[39] K. K. Kim *et al.*, "Synthesis and characterization of hexagonal boron nitride film as a dielectric layer for graphene devices," *ACS nano*, vol. 6, no. 10, pp. 8583–8590, 2012.
[40] V. Ariel and A. Natan, "Electron effective mass in graphene," in *2013 Int. Conf. on Electromagnetics in Advanced Applications (ICEAA)*, Sept 2013, pp. 696–698.
[41] S. V. Morozov *et al.*, "Giant intrinsic carrier mobilities in graphene and its bilayer," *Phys. Rev. Lett.*, vol. 100, p. 016602, Jan 2008.
[42] V. N. Kotov, B. Uchoa, V. M. Pereira, F. Guinea, and A. H. C. Neto, "Electron-electron interactions in graphene: Current status and perspectives," *Rev. Mod. Phys.*, vol. 84, no. 3, p. 1067, 2012.
[43] L. M. Woods and G. D. Mahan, "Electron-phonon effects in graphene and armchair (10, 10) single-wall carbon nanotubes," *Phys. Rev. B*, vol. 61, no. 16, p. 10651, 2000.
[44] Z. Fang *et al.*, "Gated tunability and hybridization of localized plasmons in nanostructured graphene," *ACS nano*, vol. 7, no. 3, pp. 2388–2395, 2013.
[45] J. Liu *et al.*, "Enhanced performance of graphene transistor with ion-gel top gate," *Carbon*, vol. 68, pp. 480–486, 2014.
[46] B. J. Kim *et al.*, "High-performance flexible graphene field effect transistors with ion gel gate dielectrics," *Nano letters*, vol. 10, no. 9, pp. 3464–3466, 2010.
[47] S.-K. Lee *et al.*, "Stretchable graphene transistors with printed dielectrics and gate electrodes," *Nano letters*, vol. 11, no. 11, pp. 4642–4646, 2011.
[48] B. J. Kim *et al.*, "Coplanar-gate transparent graphene transistors and inverters on plastic," *Acs Nano*, vol. 6, no. 10, pp. 8646–8651, 2012.
[49] F. Cardarelli, *Materials handbook: a concise desktop reference*. London : Springer, 2008.

Christian Nuñez Alvarez (S'14, M'16) received the B.Eng and the M.Sc degree in Telecommunications Engineering from the Technical University of Catalonia, Spain, in 2010. He has recently finished his PhD degree in Electrical Engineering at the University of Edinburgh. He is now a Research Associate in radio propagation analysis for wireless sensor networks at the University of Edinburgh, UK. His research interests are on implementing novel materials on reconfigurable antennas and signal processing in sensor networks.

Rebecca Cheung (M'96, SM'02) received first class honours and Ph.D degrees in Electronics and Electrical Engineering from the University of Glasgow, U.K., in 1986 and 1990, respectively. She currently holds a Chair in Nanoelectronics in the School of Engineering at the University of Edinburgh, U.K. Professor Cheung has an international reputation for her contribution in the development and application of micro- and nano-fabrication. She has published over 200 scientific articles, 1 patent and 1 book in related topics.

John S. Thompson (S'94, M'96, SM'13, F'16) is currently a Professor at the University of Edinburgh. He specializes in antenna array processing, cooperative communication systems and energy efficient communications. He has published in over three hundred papers on these topics, He is currently coordinator for the EU Marie Curie Training Network ADVANTAGE on the smart grid. He is an editor for the Communications Magazine Green Series. In January 2016, he was elevated to Fellow of the IEEE for contributions to antenna arrays and relay communications.